



Shape and origin of the East-Alpine slab constrained by the ALPASS teleseismic model

Ulrike Mitterbauer^a, Michael Behm^b, Ewald Brückl^{c,*}, Regina Lippitsch^d, Alexander Guterch^e, G. Randy Keller^f, Elena Koslovskaya^g, Eva-Maria Rumpfhuber^f, Franjo Šumanovac^h

^a Central Institute for Meteorology and Geodynamics, Vienna, Austria

^b Department of Meteorology and Geophysics, University of Vienna, Austria

^c Institute of Geodesy and Geophysics, Vienna University of Technology, Vienna, Austria

^d OMV, Vienna, Austria

^e Institute of Geophysics, Polish Academy of Sciences, Warsaw, Poland

^f School of Geology and Geophysics, University of Oklahoma, Norman, OK, USA

^g Sodankyla Geophysical Observatory, University of Oulu, Oulu, Finland

^h Faculty of Mining, Geology and Petroleum Engineering, University of Zagreb, Zagreb, Croatia

ARTICLE INFO

Article history:

Received 22 March 2011

Received in revised form 30 June 2011

Accepted 3 July 2011

Available online 12 July 2011

Keywords:

Teleseismic tomography

Eastern Alps

Pannonian fragment

Upper mantle structure

Subduction

Extrusion

ABSTRACT

During the last two decades teleseismic studies yielded valuable information on the structure of the upper mantle below the Alpine–Mediterranean area. Subducted oceanic lithosphere forms a broad anomaly resting on but not penetrating the 670 km discontinuity. More shallow slabs imaged below the Alpine arc are interpreted as subducted continental lower lithosphere. Substantial advances in our understanding of past and active tectonic processes have been achieved due to these results. However, important issues like the polarity of subduction under the Eastern Alps and the slab geometry at the transition to the Pannonian realm are still under debate. The ALPASS teleseismic experiment was designed to address these open questions. Teleseismic waveforms from 80 earthquakes recorded at 75 temporary and 79 permanent stations were collected during 2005 and 2006. From these data, a tomographic image of the upper mantle was generated between 60 km and 500 km depth. Crustal corrections, additional station terms, and ray bending caused by the velocity perturbations were considered. A steeply to vertically dipping “shallow slab” below the Eastern Alps is clearly resolved down to a depth of ~250 km. It is interpreted as European lower lithosphere detached from the crust and subducted during post-collision convergence between Adria and Europe. Below the Pannonian realm low velocities or high mantle temperatures prevail down to ~300 km depth, consistent with the concept of a Pannonian lithospheric fragment, which underwent strike-slip deformation relative to the European plate and extension during the post-collision phase of the Alpine orogeny. Between 350 km and 400 km depth, a “deep slab” extends from below the central Eastern Alps to under the Pannonian realm. It is interpreted as subducted lithosphere of the Alpine Tethys. At greater depth, there is a continuous transition to the high velocity anomaly above the 670 km discontinuity.

© 2011 Elsevier B.V. All rights reserved.

1. Introduction

Actual plate tectonic processes can be better understood by imaging the lithosphere and upper mantle using seismic tomography. Downgoing slabs of low temperature oceanic lithosphere and continental lithospheric mantle may be represented by bodies of relatively high seismic velocity, whereas low velocity areas may be related to areas of thinning crust and upwelling asthenosphere, mantle plumes or local mantle convection. In the Alpine–Mediterranean

area, the complex history of tectonic movements between Africa and Europe (e.g., Dewey et al., 1973; Moores and Twiss, 1995) left its trace in the upper mantle. The spreading of the North and Central Atlantic Oceans and the closure of the PaleoTethys (~190 Ma) Ocean led to a sequence of rifting, break up of continental blocks, seafloor spreading, subduction of oceanic and continental lithosphere, and re-amalgamation and suturing of micro-plates (e.g., Le Pichon et al., 1988; Stampfli and Kozur, 2006).

In the area that is the target of this study (Fig. 1), the opening and closure of the Meliata and Vardar Oceans in the south and the Alpine Tethys (Piemont–Ligurian Ocean, Penninic Ocean) in the north strongly influenced the development of the Eastern Alps and the adjoining Carpathians, Dinarides and Southern Alps. An early orogenic phase, the Eo-Alpine orogeny, occurred after the subduction of the

* Corresponding author at: Institute of Geodesy and Geophysics, Vienna University of Technology, Gusshausstrasse 27-29/1282, A-1040 Vienna, Austria. Tel.: +43 1 58801/12820; fax: +43 1 58801/12892.

E-mail address: ebrueckl@mail.tuwien.ac.at (E. Brückl).

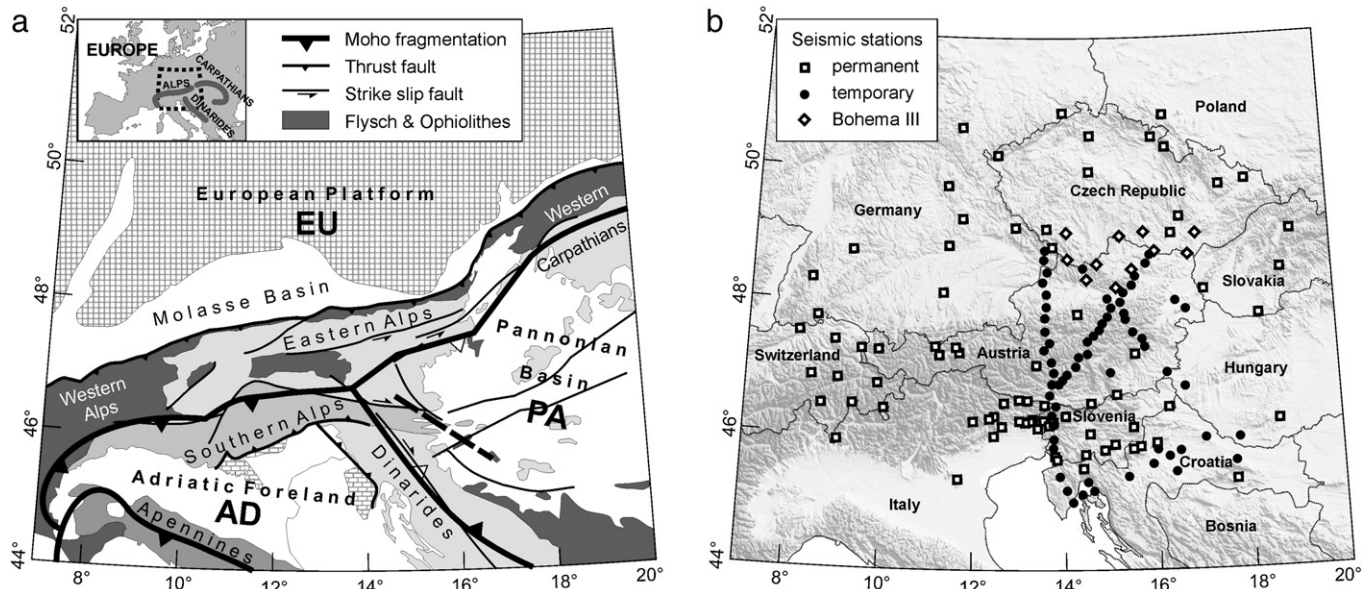


Fig. 1. Tectonic setting of the study area and locations of the seismic network. a) Geological map shows the main tectonic units and major faults; Flysch belts and ophiolites are mapped in dark gray; the Moho fragmentation (after Waldhauser et al., 1998 and Brückl et al., 2010) is plotted by bold lines; triangles indicate thrust polarity. b) Location of temporary ALPASS stations (spheres), seismic observatories (squares), and BOHEMA III stations (diamonds).

Meliata Ocean from 130 to 85 Ma. Seafloor spreading of the Alpine Tethys ended at about 130 Ma and subduction of this ocean was initiated ~80 Ma with Europe representing a passive margin. The Adriatic micro-plate or Adria started to move independently from Africa to the NW, and at ~35 Ma, it collided with Europe (e.g., Schmid et al., 2004). In the Oligocene (35–30 Ma), a slab break off occurred (Wortel and Spakman, 2000) in the central part of the Eastern Alps. During the Miocene, retreat of the remaining Alpine Tethys into the Carpathian embayment led to the development of the Pannonian basin and subsequently the Carpathians (e.g., Royden, 1993). The Apennines and Dinarides (e.g., Doglioni and Carminati, 2002; Horváth et al., 2006; Pamić et al., 2002) formed by subduction of Adriatic continental mantle to the west and the east. Major blocks of the East Alpine region (ALCAPA) extruded laterally to the east into the Carpathian embayment (Decker and Peresson, 1996; Linzer et al., 2002; Ratschbacher et al., 1991a,b) (Fig. 1). These units experienced significant extension, before their final collision with the Paleozoic European platform, which formed the Western Carpathians (Ustaszewski et al., 2008).

The Hellenic arc represents the currently most active area related to the continued convergence between Africa and Europe. Global and large scale tomographic models (e.g., Bijwaard et al., 1998; Piromallo and Morelli, 2003; Wortel and Spakman, 2000) show a slab subducting into the upper mantle of the Alpine region and suggest penetration of the 670 km discontinuity. Between the 410 km and 670 km mantle discontinuities, an extensive region of relatively high seismic velocities exists underneath the Pannonian basin and the surrounding Alpine–Carpathian–Dinaric orogens. This zone is interpreted as the remnants of subducted oceanic plates (e.g., Vardar, Meliata, NeoTethys, Alpine Tethys or Piemont and Ligurian Ocean) and will be referred to as the “slab graveyard”. Our use of this term should not be confused with cold subducted lithosphere, which is interpreted to have sunk to form a “slab graveyard” at the core–mantle boundary (e.g., Tackley, in press). Ps receiver functions derived from observatory data in central and eastern Europe yield high travel time differences between the 410 km and 670 km arrival and give additional support for the existence of the slab graveyard (Geissler et al., 2008). Shallower slabs are resolved for instance underneath the Alpine arc, the Apennines and the Dinarides. Paleogeographic reconstructions have shown that there is a balance

between the volume of all these high velocity bodies and the volume of subducted dense and cold lithosphere (Handy et al., 2010).

A high-resolution tomographic image of the Alpine slab, extending from the Moho discontinuity to 400 km depth was provided by Lippitsch et al. (2003). The southward oriented dip of the slab in the Western Alps showed European lower lithosphere subducting underneath Adria. The lateral continuity of the slab appears reduced to the east, and further to the east, a pronounced north-dipping (~60°) slab was imaged. These results led to the interpretation of a subduction polarity change from west to east under the Eastern Alps. These findings have greatly influenced tectonic interpretations of the region (e.g., Horváth et al., 2006; Kissling et al., 2006; Schmid et al., 2004, 2008; Ustaszewski et al., 2008). However, more recent results are in conflict with these tectonic interpretations and favor the more “classical” interpretation of subduction of the European plate (EU) under the Adriatic plate (AD) along the whole Alpine arc and subduction of the Adriatic plate only under the Dinarides and Apennines (Doglioni and Carminati, 2002). Arguments for the more “classical” interpretation include the interpretation of the crustal structure along the TRANSALP transect by Lammerer and Weger (2008) and the Moho fragmentation and plate kinematics at the bifurcation of subduction via a triple junction between the European, Pannonian (PA), Adriatic lithospheric blocks (Brückl et al., 2010). The fragmentation of the Moho and the uppermost mantle into AD, EU, and PA blocks is superimposed on Fig. 1. The pattern of the fragmentation and the polarity of thrusting follow Brückl et al. (2010) in the Eastern Alps and northern Dinarides. In the Western Alps and Apennines, the boundaries between the European, Adriatic, and Ligurian plates follow the Moho map of Waldhauser et al. (1998). Šumanovac (2010) employed gravimetric modeling to delineate a significant Moho jump under the Dinarides. This result was implemented to extend the Moho fragmentation between EU and PA further to the south (Fig. 1a).

2. The ALPASS project

The ALPASS (Alpine Lithosphere and Upper Mantle PASSive Seismic Monitoring; <http://info.tuwien.ac.at/geophysik/alpass.htm>) project is an international effort to supply new data in the Eastern Alps and their neighboring tectonic provinces. This project has been a

cooperation between geophysical institutes from Austria, Croatia, Finland, Poland and USA. The ALPASS array was specifically designed to determine subducting slab geometries in the Eastern Alps–Pannonian–Carpathian (ALPACA) region and to address or even clarify the issues of the polarity of subduction below the central part of the Eastern Alps.

In this study, teleseismic tomography using ALPASS and regional data (Fig. 1b) was employed to produce a high-resolution image of the upper mantle below the Eastern Alps. The resulting model overlapped the model of Lippitsch et al. (2003) and extended further to the east. In our analysis, we took advantage of the most recent crustal models (e.g. Behm et al., 2007; Brückl et al., 2007; Grad et al., 2009a,b; Šumanovac et al., 2009) derived from CELEBRATION 2000, ALP 2002 and SUDETES 2003 (Guterch et al., 2003) controlled source seismic data. As shown below, our tomographic results were compared with the large scale tomographic model of Koulakov et al. (2009) and the model of Lippitsch et al. (2003) in the area overlapping with ALPASS. Most recent tomographic results, based on the CBP (Carpathian Basin Project) data (Dando, 2010; Dando et al., 2011; Houseman et al., 2010) and a geodynamic model (Brückl et al., 2010) of the East Alpine area supplied additional support for the interpretations presented here.

3. Travel time picking and crustal corrections

Between May 2005 and May 2006, seismic waveforms from 80 earthquakes in the teleseismic distance range (30°–100°) were collected from 79 seismic observatories and 64 temporary seismic stations during the ALPASS experiment. Additional seismic wave-

forms from 11 temporary seismic stations in the area of the Bohemian Massif were added through data exchange with the BOHEMA III project (Babuška et al., 2005). A generalized tectonic map and the locations of the seismic observatories and temporary stations employed are shown in Fig. 1a and b. Epicenters of the evaluated earthquakes, their azimuth distribution around the investigation area, and the frequency distributions of magnitudes and distances are plotted in Fig. 2. Each of the 154 seismic stations and observatories shown in Fig. 1b recorded at least 10 earthquakes with sufficient quality for further evaluation.

Seismic recordings were transformed to the short period response WWSSN-SP (World Wide Standard Seismic Network) and reduced to ak135 travel times (Kennett et al., 1995), at a focal depth 15 km (Fig. 3a). Cross-correlation and adaptive stacking techniques support high quality estimation of travel time residuals across a seismic network (e.g., Rawlinson and Kennett, 2004). We chose an interactive procedure employing the seismic data processing software ProMAX (Halliburton). The processing sequence is illustrated by the flow chart shown in Fig. 3a. Reference traces for each event were generated by stacking after alignment to automatically picked first arrivals. Cross-correlation of the individual traces with a 15 s window of the reference trace (Fig. 3b) yielded a first estimate of travel time differences between the traces. These travel time differences were used for improved alignment and stacking of the reference trace. Cross-correlation using a 4 s window of the reference trace (Fig. 3c) was then centered on the first onset and provided accurate travel time residuals (Fig. 3d, e). The procedure was repeated if the stack of the reference trace was of low quality. Next, the results were manually inspected, a signal to noise ratio was determined automatically, and

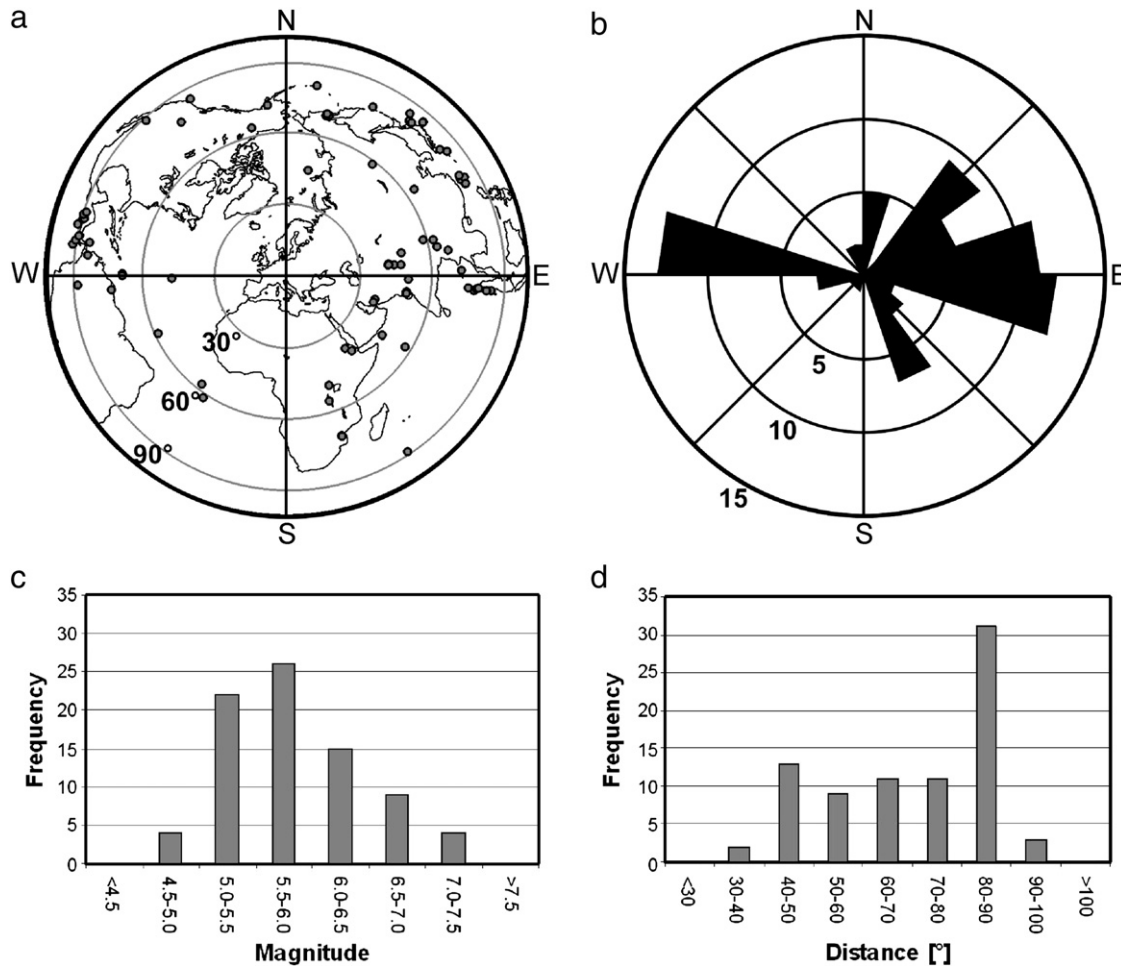


Fig. 2. Earthquake data. a) Location of epicenters (80 earthquakes). b) Azimuth distribution of epicenters. c) Frequency of magnitudes. d) Frequency of distances.

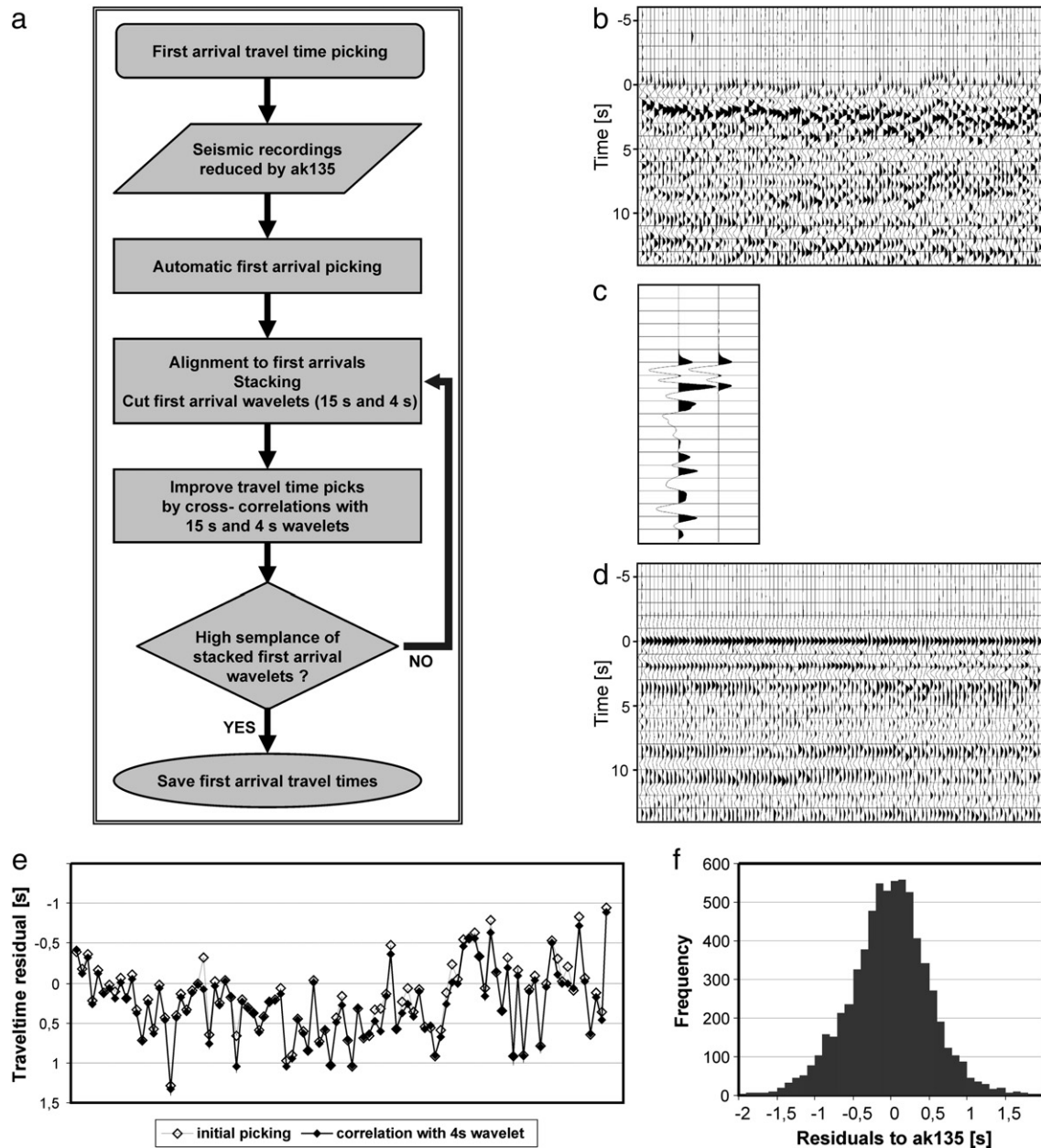


Fig. 3. Travel time picking. a) Flow chart of travel time picking procedure. b) Records of the 14 June 2005, M6.7 Andreanov Islands earthquake, transformed to WWSSN-SP response, reduced by ak135 travel times, traces are sorted to increasing epicenter distances from left to right. c) 15 s and 4 s correlation wavelets derived from records shown in b). d) Same data; correlation with 4 s wavelet; traces are aligned according final travel time picks. e) Initial and final picks of travel time residuals. f) Frequency distribution of travel time residuals (6634 picks, standard deviation 0.558 s).

low quality traces were removed. A total of 6634 P-wave travel time residuals were picked by this method. Their frequency distribution is shown in Fig. 3f.

Resolution of upper-mantle structure by seismic tomography depends critically on information of the crustal velocity structure beneath the receiver array (e.g., Koulakov et al., 2009; Lippitsch et al., 2003). A-priori information is necessary to resolve areas with highly variable crustal structure, since the ray geometry from teleseismic sources is not appropriate to resolve these layers with sufficient resolution. The Alpine region is well known for its complex crustal structure and station corrections are on the order of seconds and vary with both back-azimuth and emergence angle (Lippitsch et al., 2003; Waldhauser et al., 2002). A 3D crustal P-wave velocity model encompassing the Eastern Alps and its surrounding area (Pannonian Basin, Dinarides, and Bohemian Massif) was compiled from the 3D seismic model of Behm et al. (2007) and the 2D seismic profiles of

Lüschen et al. (2006), Brückl et al. (2007), Grad et al. (2006, 2009b), Hrubcova et al. (2005, 2008), and Šumanovac et al. (2009) in the east and Waldhauser et al. (1998) in the west. The model extends to a depth of 60 km, and first order discontinuities such as the Moho topography, sedimentary basins, and strong intra-crustal velocity anomalies were included.

Crustal corrections for the P-wave arrivals were calculated with the program Tetra3D (Waldhauser et al., 2002). The result is a continuous travel time field for each teleseismic event, which provides information on the contribution of the 3D crustal structure on the total travel time for each seismic event and each station. After correction for the 3D crustal structure, the residuals mainly contain information on travel time differences through the upper mantle beneath the Alpine region. This same methodology for crustal corrections was applied by Lippitsch et al., 2003 to the Western Alps. Corrections for station elevation were also applied. Average

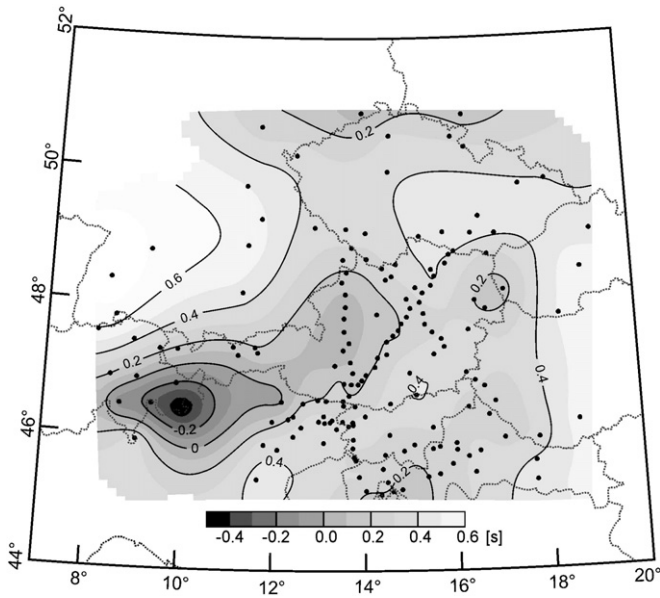


Fig. 4. Average crustal corrections. Crustal corrections were calculated for each receiver station (spheres) and earthquake; gray scale and contour lines visualize average of crustal corrections for each station.

crustal corrections for the seismic stations are plotted in Fig. 4. These values vary from -0.526 s (Central Alps) to $+0.773$ s (Pannonian Basin, Rhine Graben) and were added to the observed travel times. Crustal corrections for a single station depend on back-azimuth to the earthquake and the angle of incidence. The standard deviation of this variation is 0.157 s on average. The error in the crustal corrections is about in the same range under the assumption of ± 2 km error in Moho depth.

4. Inversion

Wave fronts propagating from earthquakes at teleseismic distances arrive nearly undisturbed at the upper mantle of the target area. Uncertainties in focal time and depth, as well as distant propagation effects can be approximated by subtracting the average of all residuals of one earthquake from the data before inversion. The ak135 global seismic model (Kennett et al., 1995) was used to reduce the travel times and crustal corrections were estimated relative to this model. The velocity field of the target area was defined on a regular 3-D grid with equidistant spacing of 30 km in all three dimensions, and a lateral extent of 1140 by 1140 km that was centered at 14.2°E and 47.9°N. The vertical extent reaches from surface to a depth of 570 km.

We used the code provided by N. Rawlinson (e.g., Rawlinson and Kennett, 2008; Rawlinson et al., 2006; <http://rses.anu.edu.au/~nick>)

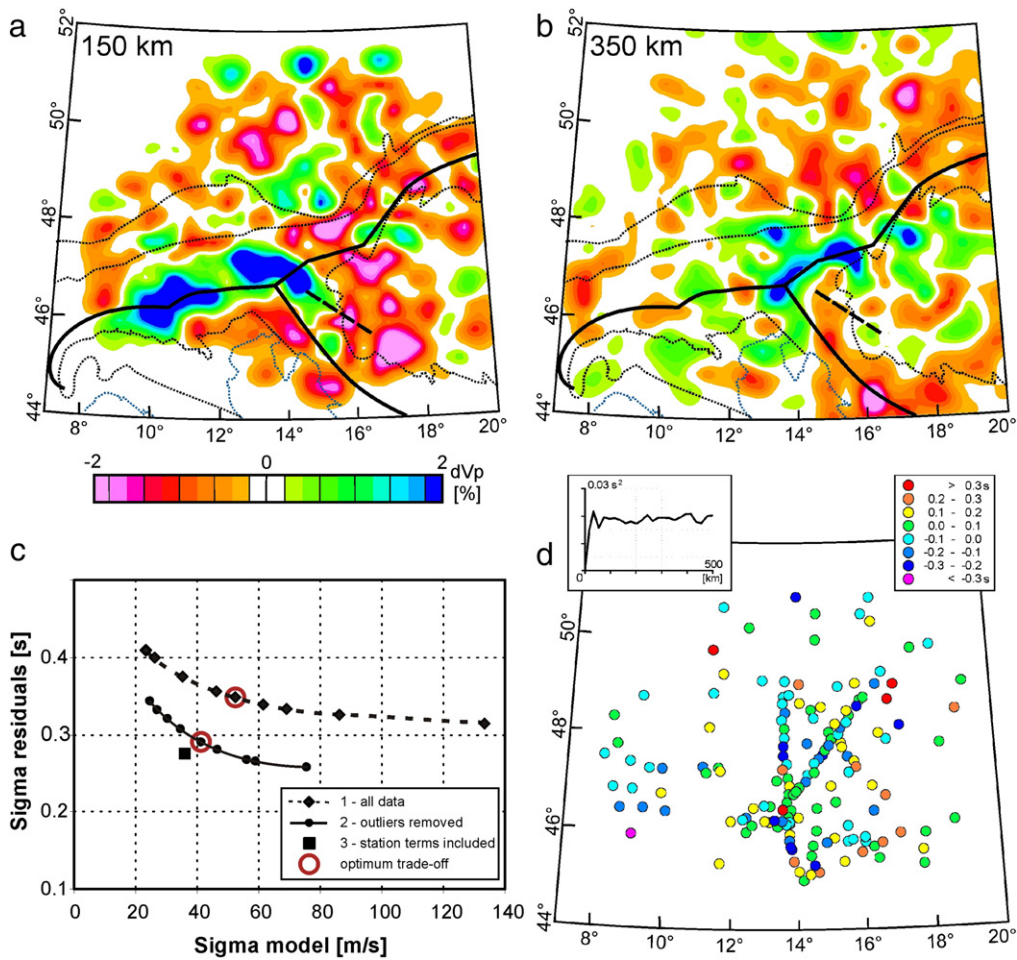


Fig. 5. Inversion approach. We started the inversion using all travel times (a, b) and applying crustal corrections. Thereafter outliers were removed. Trade-off curves (c) supported an appropriate choice of smoothing and damping factors. Finally station terms were applied. Significant spatial correlation between the station terms (d) was suppressed by an additional damping factor. a) Depth slice 150 km: inversion using all times, crustal corrections, no smoothing ($\epsilon = 0$), damping factor $\mu = 1$; b) Depth slice 350 km: inversion using all travel times, crustal corrections, no smoothing ($\epsilon = 0$), damping factor $\mu = 5$; c) RMS of travel time residuals versus model roughness. 1 – trade-off curve for all travel times ($\epsilon = 0, 100 \geq \mu \geq 0.5$, optimum $\mu = 15$ is marked by red circle); 2 – trade-off curve for travel time data with outliers removed ($\mu = 2, 300 \geq \epsilon \geq 0$, optimum $\epsilon = 50$ is marked by red circle); 3 – further optimization by consideration of station terms (damping of station terms $\nu = 600, \mu = 2, \epsilon = 50$). d) Station terms: the variogram (inset) demonstrates the lack of spatial correlation between station terms.

for the residual travel time inversion. Travel times from teleseismic events were computed to the base of the local 3-D model using the ak135 model, which was also used as initial model within the target area. An eikonal solver, based on the fast marching method (de Kool et al., 2006) was implemented in order to compute travel times and ray paths through the local 3-D model. The differences between the observed and the calculated travel times were inverted for velocity perturbations along the ray paths in the 3-D model. This procedure was repeated iteratively such that, at each step, travel times and ray paths are calculated in the updated velocity model down to its base. From this level through the mantle to the hypocentre, a 1D solution derived from the ak135 model was taken. The instability of the inversion problem was overcome by the introduction of damping and smoothing factors. Both parameters control the trade off between the smoothness of the solution and the data fit. Their actual choice depends on the number of grid nodes and observations, the estimated picking accuracy and the overall ray coverage. Output of the inversion is a 3-D model of velocity changes relative to the ak135 model at greater depths than the crustal model (60 km).

The results of an initial inversion using the complete travel time data set with crustal corrections are shown in Fig. 5a and b by horizontal slices through the inverted velocity perturbation at 150 km and 350 km depth. The smoothing factor was set $\varepsilon=0$ and the damping factor $\mu=15$ determined by the trade-off curve 1 shown in

Fig. 5c. The number of iterations was set to 4 and remained unchanged for all inversions. The standard deviation of the residuals is 0.348 s, which corresponds to a variance reduction to 39% compared to the initial standard deviation of 0.558 s. A closer look at the residuals shows that certain travel times have large residuals in all inversions, which is indicative of outliers in the data set. In order to remove outliers we defined a boundary of 2.5 times the standard deviation of the residuals and rejected all travel times that had a residual larger than this limit (0.87 s). The travel time data set was reduced to 6368 observations by applying these criteria (266 observations were eliminated). The standard deviation of the original travel time data set was reduced from 0.558 s to 0.518 s by the elimination of outliers. The trade-off curve 2 in Fig. 5c was used to determine an optimum smoothing factor of $\varepsilon=50$ in combination with a damping factor of $\mu=2$ for the reduced data set. In addition, the code by Rawlinson allows for the determination of static corrections (or station terms), in order to compensate for near surface effects below the seismic stations. An additional damping factor (ν) stabilizes the determination of these station terms (Fig. 5d). We chose the damping factor for the static correction $\nu=600$ and kept $\mu=2$ and $\varepsilon=50$ (Fig. 5c). A lower value of ν did not significantly reduce the travel time residuals. The relatively high damping guaranteed also that the station terms represent only local velocity perturbations with no wider spatial correlation. This has been verified by a variogram of the station terms

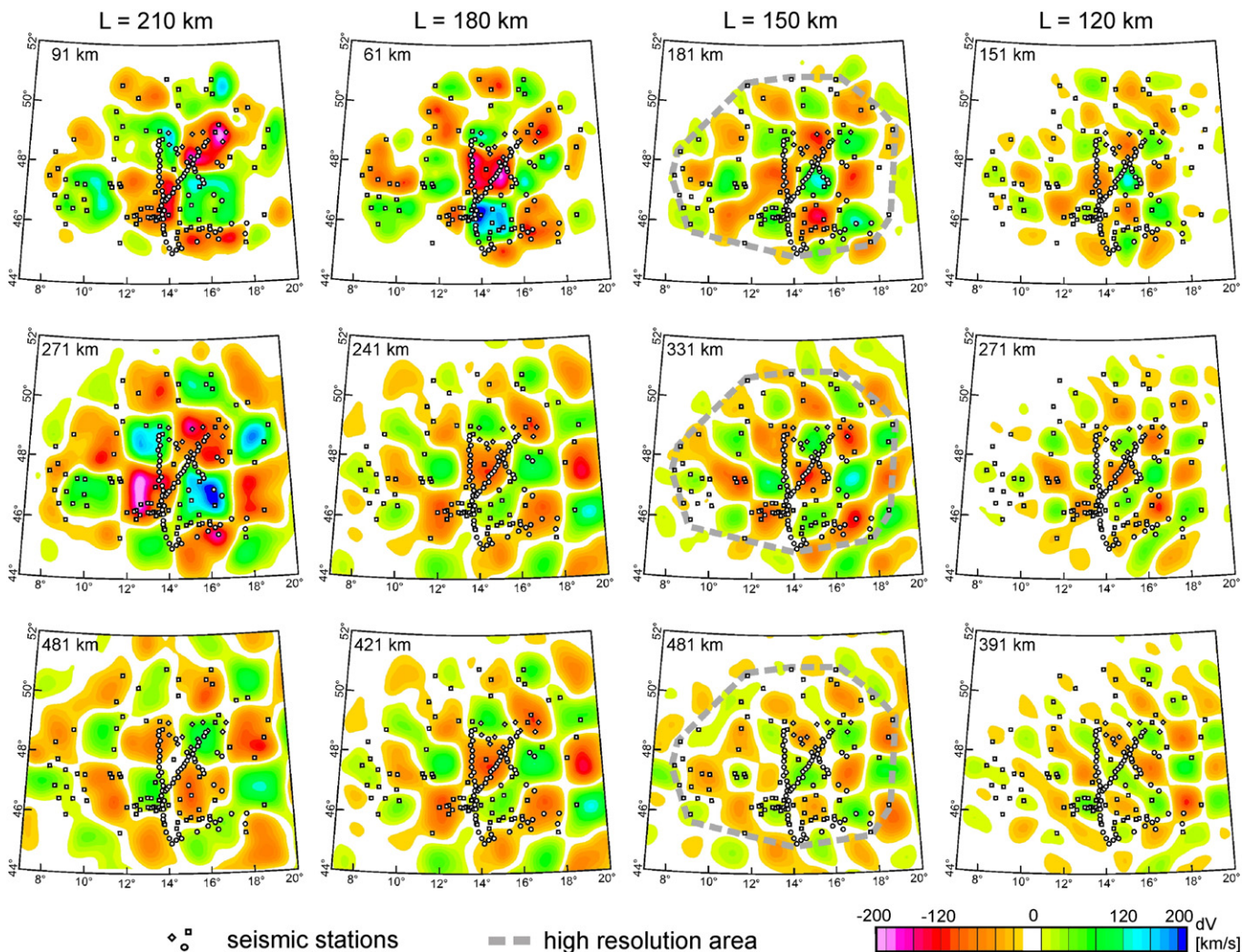


Fig. 6. Resolution tests. Positive and negative velocity anomalies (± 200 km/s) were superimposed in a checkerboard pattern on the ak135 model and recovered by an inversion with $\mu=15$ and $\varepsilon=50$; cell length of one checker (L) varies from 120 to 210 km; the dashed circular feature around seismic stations in the $L=150$ km column approximates the high resolution area we have emphasized.

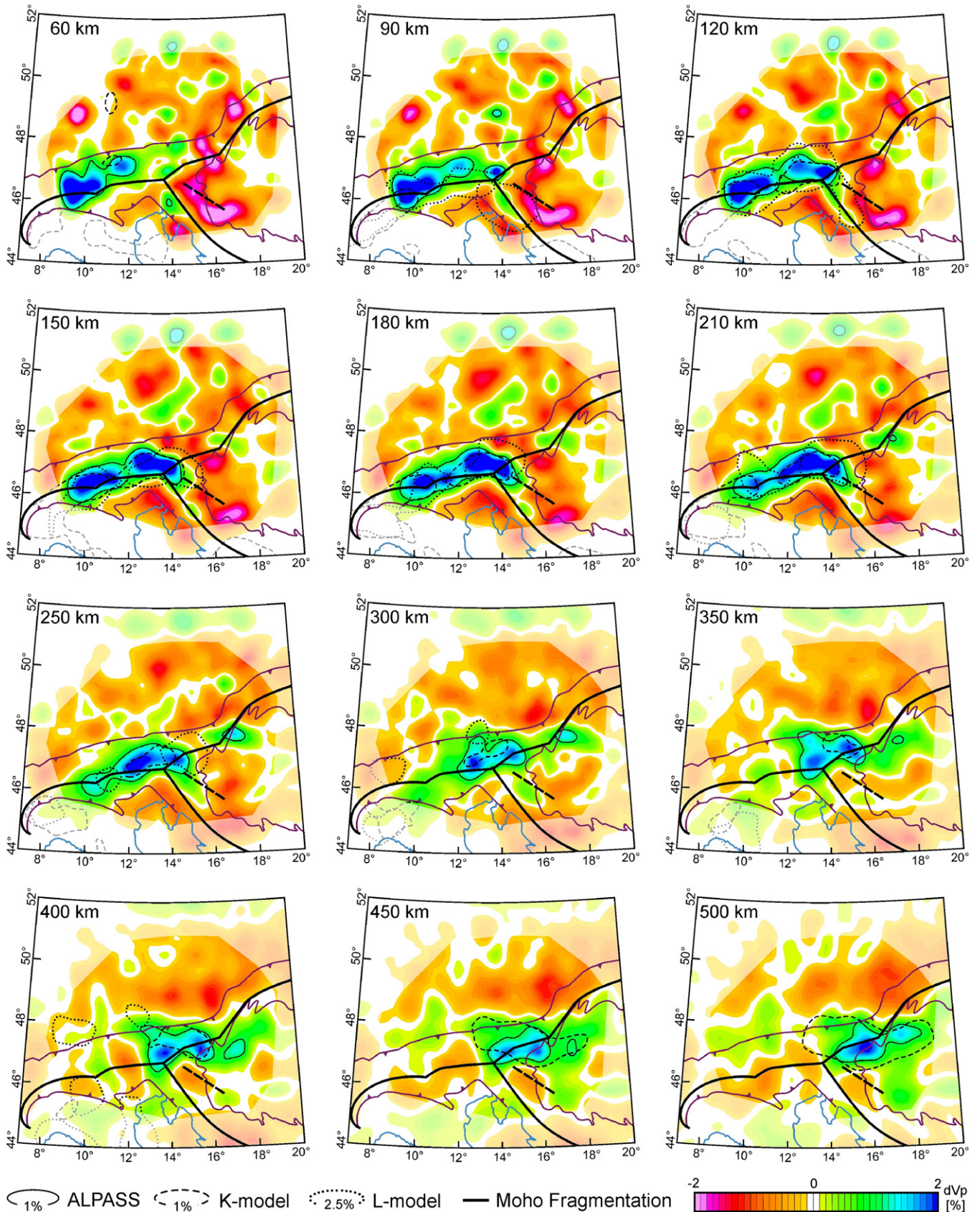


Fig. 7. Depth slices through ALPASS-model from 60 km to 500 km depth. The velocity anomalies relative to the ak135-model are visualized by color; the + 1% contours are medium black lines that separate the light blue and green areas; outside the high resolution area, the colors are pale. For comparison of the ALPASS model with existing models, + 1% contours of the K-model are shown as medium dashed black lines (Koulakov et al., 2009) and + 2.5% contours of the L-model are shown as medium dotted black lines (Lippitsch et al., 2003). Superimposed on the depth slices are coastlines (blue lines), the outline of the Pannonian basin, and the northern and southern thrust faults of the Alpine orogen (pink lines, the thrust faults with signatures indicating the polarity). Similar to Fig. 1 the Moho fragmentation is shown by thick black lines, and a subdivision within the Pannonian fragment as a short dashed line.

shown by the inset in Fig. 5d. The standard deviation of the travel time residuals was reduced to 0.275 s by the final model. The final model will be discussed below. However, the main features of the model were clear even in the initial inversion using all travel times, zero smoothing, and no station terms. Even omitting the crustal corrections did not substantially change the seismic image at greater depths, but slightly increased the remaining travel time residuals.

Checkerboard tests (e.g., Hearn and Ni, 1994) are a commonly used technique to analyze the resolution capabilities of tomographic inversions. We superimposed velocity anomalies of ± 0.2 km/s on the ak135 model, and calculated a set of synthetic travel times. Gaussian noise with a standard deviation of 0.2 s was added to the travel times, and they were inverted with the same parameters as used in the final inversion of the observed travel times. The size of the checkers was varied between 300 and 30 km, and Fig. 6 shows the

most important results. A convex boundary enclosing the seismic stations and observatories was superimposed on the reconstructions. In general, the resolvability varies with both checker size and depth. We chose to interpret the checker size of $L = 150$ km, since it appears as the most representative with respect to the structures. We further took the boundary enclosing all the seismic stations and observatories (Fig. 6) as a conservative delimitation of the high-resolution area and restricted our interpretations accordingly.

5. Results

The 3D P-wave velocity model derived by our analysis is presented by a series of depth slices between 60 km and 500 km depth (Fig. 7). Vertical profiles crossing the Alps arc approximately orthogonally to its strike direction are shown in Fig. 8. We will concentrate on the

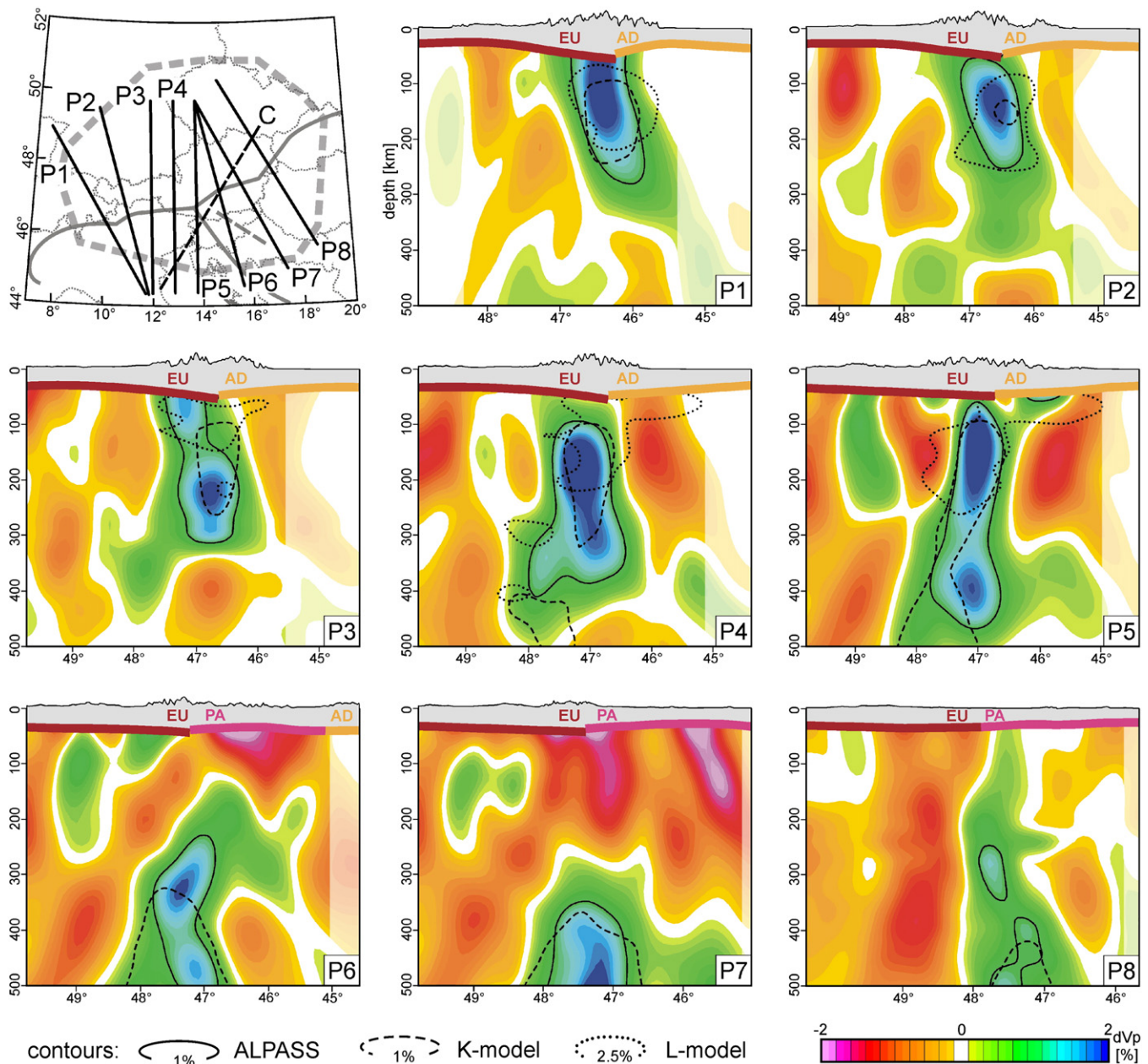


Fig. 8. Profiles through the ALPASS-model. The velocity anomalies are visualized in color similar to Fig. 7. Superimposed on each profile is a crustal model with Moho after Behm et al. (2007), Grad et al. (2009a), Waldhauser et al. (1998), and Brückl et al. (2010). Topography is 10-times vertically exaggerated; for comparison of the ALPASS model with existing models contours of the K- and L-models (Koulakov et al., 2009; Lippitsch et al., 2003) are also shown (medium dashed and dotted lines respectively). The map of the profiles (P1–P8) including the extent of the high resolution area of the ALPASS-model (bold dashed gray boundary) and the Moho fragmentation (bold gray lines) are shown in the upper left corner.

main structures visible on the depth slices, which were robust independent of the choice of inversion parameters and travel time errors. This can be checked by comparison of the results of the initial inversion shown in Fig. 5 with the corresponding depth slices through the final model shown in Fig. 7. A high velocity body extends from the western border of resolution of the ALPASS-model (9°–10°E) to ~15°E under the Alpine arc at the depth levels from 60 km to 250 km, which we will refer to as the “shallow slab”. This feature was recognized earlier by global seismic tomography studies (Bijwaard et al., 1998; Piromallo and Morelli, 2003) and resolved by the models of Lippitsch et al. (2003) and Koulakov et al. (2009). These latter models will be referred to as the L- and K-models respectively. Contour lines of L- and K-models fit our new model well (Fig. 7). The shallow slab is bordered by low velocity zones to the NE, SE and the Pannonian basin, indicating higher temperatures in the upper mantle.

Around 300 km depth, the velocity pattern changes configuration. A high velocity body is well resolved from 350 km to 450 km depth around ~47°N latitude. This body, which will be referred to as “deep slab”, begins in the west at ~13°E and extends near to the eastern resolution border of the ALPASS-model. It is imaged by the K-model as well, and furthermore, Dando (2010) delineated this slab by teleseismic tomography based on data from the CBP-project (Dando et al., 2011; Houseman et al., 2010). Additional support for the existence of high velocity mantle above the 410 km mantle discontinuity is supplied by receiver functions, which have piercing points in the area of the “deep slab” (Kummerow et al., 2004). The L-model does not extend as deep and far enough to the east to resolve this high velocity body.

At greater depth (~500 km) high velocities prevail in the wider Pannonian area. This is the level of the slab graveyard (e.g., Handy et al., 2010), which has been imaged by global and large-scale tomographic models (e.g., Bijwaard et al., 1998; Piromallo and Morelli, 2003; Koulakov et al., 2009). However, despite the fact that checkerboard tests indicate good resolution in a wider area, the ALPASS-model can only resolve the slab graveyard in a restricted area around the transition from the Eastern Alps to the Pannonian basin.

Profiles P1–P5 (Fig. 8) cross the shallow slab approximately in its dip direction. Its shallowest section (depth ~60 km) is connected to the southern end of the European Moho. In the west (profile P1) the shallow slab dips slightly to the south (~80°), further to the east (profiles P2 to P5), the slab dips sub-vertically. In the west, from profile P1 to P3, significantly higher velocities reach down to depth of ~250 km. Profiles P4 and P5 indicate that there is a possibility for the shallow slab to be connected to the deep slab, which begins at about 300 km depth. Profiles P6, P7, and P8 cross the Eastern Alps east of the extent of the shallow slab and show only the deep slab. The low velocity, high temperature zone under the Pannonian fragment is

significantly developed along profiles P6 and P7. The contours of the K- and L-models, which are superimposed on the profiles, confirm the general shape of the shallow slab. On profile P3, the L-model indicates a reduced continuity of the shallow slab from west to east more distinctly than the images provided by the ALPASS-model and K-models. As mentioned earlier, because of its reduced depth extent, the L-model does not show the deeper part of the slab. The continuous transition from the deep slab to the slab graveyard between 400 km and 500 km depth is best shown by the K-model, because it has the greatest depth extent.

6. Interpretation and discussion

Fig. 9 shows cross sections through the K-, L-, and ALPASS-models along the SW–NE directed profile C of Lippitsch et al. (2003) across the Eastern Alps (see map in Fig. 8). The northern part of profile C is situated on European lithosphere. Between the latitudes 47.3° and 46.5°, the profile crosses the Pannonian fragment parallel and near to the boundary between Pannonian and European lithospheres. South of the latitude 46.5°, profile C is on Adriatic lithosphere. At shallow depth <100 km the L-model displays high velocity lithospheric mantle below the Adriatic Moho. The K- and ALPASS-models do not show this feature clearly. Differences in crustal corrections between the three models could explain this discrepancy. All three models image the shallow slab below the Pannonian Moho. The cross sections through the K-model and ALPASS-model show a steeply (more than 80°) north dipping shallow slab extending to about 250 km depth and its transition to the deep slab below 300 km depth. In contrast to these models, the L-model illustrates an ~60° north-dipping shallow slab, and as discussed earlier, no deep slab. The L-model (Lippitsch et al., 2003), especially profile C, led to the interpretation of a change of dip polarity from the European Plate (EU) under the Adriatic plate/Adria (AD) in the west to AD subducting under EU in the east at about ~12°E, the location of the reduced continuity of the shallow slab (e.g., Kissling et al., 2006; Lippitsch et al., 2003; Schmid et al., 2004). This dip polarity change to the east is explained by the assumption that AD continental lower lithosphere subducted to the northeast under the Dinarides during Eocene orogenesis. Former subducted Meliata Ocean lithosphere diverted the AD slab underneath the Tauern window, the location where it has been actually resolved by the tomographic models. However, because of the strong evidence for the deep slab given by the ALPASS-, K-, and CBP-models, the few seismic stations implemented into the L-model east of ~14°E, and its limited depth extent, we believe the new tomographic images of the ALPASS-, and K-models are more representative than the L-model in this area. We assume that the implementation of a deep slab as a high velocity body

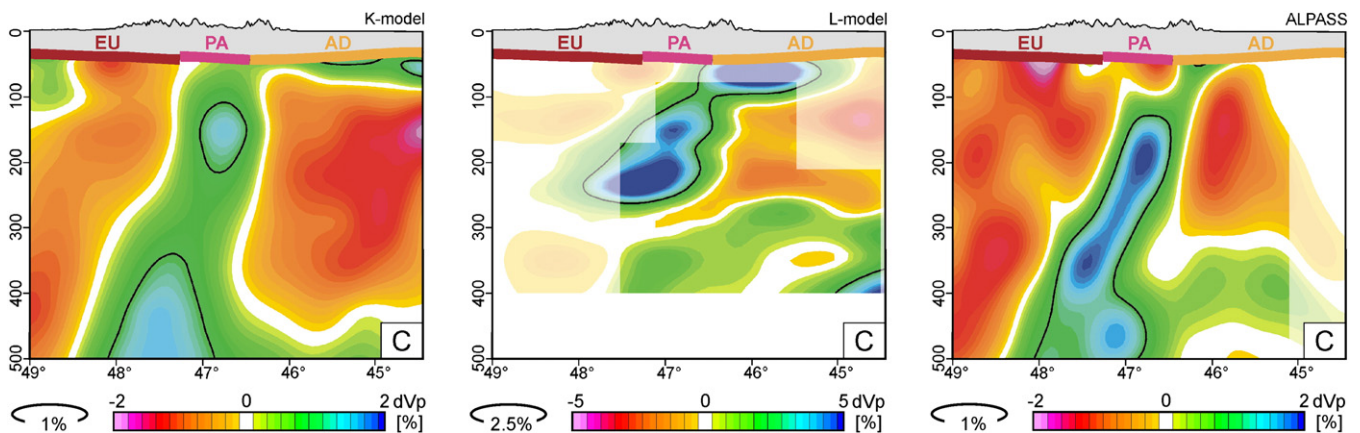


Fig. 9. Comparison of the K-, L-, and ALPASS-models along profile C. Location of profile C (Lippitsch et al., 2003) is shown in the map in the upper left corner of Fig. 8; the velocity anomalies are visualized in color similar to Fig. 7, the crustal model similar to Fig. 8.

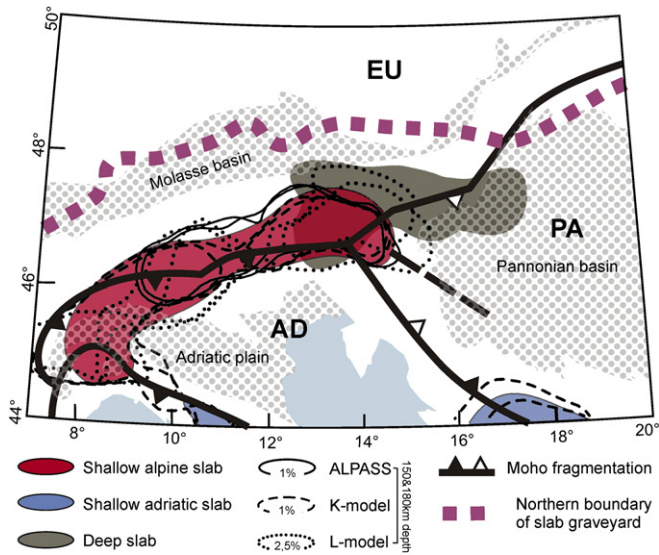


Fig. 10. Synopsis of structural features from surface to 670 km discontinuity. The Adriatic and Ligurian Sea (light blue areas) and the Molasse, Pannonian, Po and Venetian basins (pattern of gray circles) represent surface features. The Moho fragmentation is shown by thick, black lines with dip signatures. The European plate, Adriatic micro-plate, and Pannonian fragment are labeled by EU, AD, and PA. Contours of the velocity anomalies at 150 km and 180 km depth of the ALPASS-model (+1%, solid lines), the K-model (+1%, dashed lines), and the L-model (+2.5%, dotted lines) show the extent of shallow slabs. An average horizontal cross section through the Alpine shallow slab at 150–180 km depth according to the ALPASS-, K-, and L-models is shown in red. Shallow Adriatic slabs imaged by the K-model under the Dinarides and Apennines are shown as dark blue areas. An average horizontal cross section at 350–400 km depth through the Alpine deep slab is marked by a gray area. The deepest structural feature above the 670 km discontinuity is the slab graveyard. Its northern border, according to Piromallo and Morelli (2003) and Handy et al. (2010), is plotted by a thick, dotted, pink line.

into the L-model would significantly change the image of the shallow slab east of $\sim 14^\circ\text{E}$.

Fig. 10 illustrates the interpretation of the observed high velocity bodies under the Eastern Alps, which was derived from our new results. The Molasse basin, Adriatic plain, and the Pannonian basin bound the Alpine, Carpathian, and Dinaric orogens at the surface. The individual tectonic blocks are separated by relatively sharp boundaries at the Moho level due to the fragmentation of the crust and uppermost mantle into AD, EU, and PA. The lateral extent of the shallow slab under the Alps is outlined according to the relative velocity contours (+1% and +2.5%) at 150 km and 180 km depth of the ALPASS-, K-, and L-models. There is agreement between all three models, and the outline of the shallow slab does not deviate more than ± 30 km from the contours of the different models. Obviously, these results are very robust and not significantly influenced by ray path distortions from the 3D velocity structure. Ray path distortions were considered only by the ALPASS- and L-models, and not the K-model.

Contours of the +1% velocity deviation at 350 km and 400 km depth of the ALPASS- and K-models represent the lateral extent of the deep slab (gray area in Fig. 10). The easternmost part of the Alpine shallow slab overlaps with the deep slab and a connection between these two slabs between 13°E and 15°E cannot be excluded. The northern rim of the slab graveyard is shown by the +0.44% relative velocity contour, which was extracted by Handy et al. (2010) from the model of Piromallo and Morelli (2003). The northern boundary of the deep slab follows this rim approximately. The K- and L-models delineate deep slabs also in the Western Alps. However, these features are beyond the scope of our study.

There is general agreement about the nature of the slab graveyard (~ 550 km depth, between the 410 km and 670 km discontinuities) as

being remnants of oceanic and lower continental lithosphere, which were subducted since the breakup of Pangea and the closure of Paleotethys (e.g., Handy et al., 2010; Wortel and Spakman, 2000). The results from the ALPASS-model confirm this large-scale structure. However, our results do not shed new light on this question. The deep slab that clearly developed below 300 km depth with a continuous transition to the slab graveyard below 450 km depth and is interpreted as a remnant of the oceanic lithosphere of the Alpine Tethys on its way down to the slab graveyard. The Moho fragmentation (Brückl et al., 2010; Waldhauser et al., 1998) supports the interpretation of the shallow slab below the Alpine arc. The axis of the shallow slab follows the Moho fragmentation in general. At longitude 10°E , the axis of the shallow slab is ~ 20 km south of the fragmentation, at 12°E just below, and at 14°E , the longitude of the triple junction AD–EU–PA, ~ 20 km north of it. The shallow slab is interpreted as EU continental lower lithosphere delaminated from EU crust. It has been subducted nearly vertically after collision between AD and EU about 35 Ma ago, thus supporting further post-collision convergence between AD and EU. A shallow slab could not be confirmed below the EU–PA boundary from the triple junction to the Western Carpathians by our new or by previous models (e.g., Dando, 2010; Dando et al., 2011; Koulakov et al., 2009; Wortel and Spakman, 2000).

The tectonic/kinematic model of Brückl et al. (2010) proposes that strike-slip dominates along the EU–PA boundary from the triple junction to the Western Carpathians (Fig. 1) because of the ongoing lateral extrusion of the Pannonian fragment to the east or northeast. If this general scheme applies to the relative movements between PA and EU since the late Oligocene, then we may infer that the EU–PA plate boundary was essentially a transform structure, and hence did not lead to the development of a shallow slab. This kinematic model also postulated extension between AD and PA near the triple junction (Fig. 1), and also transpression south of 46°N (Fig. 1). Again, this mechanism does not allow for the development of a shallow slab at the AD–PA plate boundary north of $\sim 45^\circ\text{N}$ after the collision. Neither our new model, nor previous models show significant bodies of cold lower lithosphere in this area. Further to the south, the K-model is in agreement with other large-scale models (e.g., Bijwaard et al., 1998; Piromallo and Morelli, 2003), which show a large shallow slab that is subvertical below the AD–PA plate boundary. This finding fits well to a kinematic scheme with a larger convergent component of relative plate movement in this area (e.g., Grenerczy and Kenyeres, 2006).

The western, northern, and southern borders of the deep slab are well defined by the new ALPASS-model, and there is good agreement with the K-model. The CBP-model shows a similar structure. Houseman et al. (2010) and Dando (2010) point out that the northern rim of the deep slab approximately follows the northern margin of ALCAPA, as reconstructed by Ustaszewski et al. (2008) for the Early Miocene. Slab break-off and roll back of the Alpine Tethys into the Carpathian embayment according to Royden (1993) or Wortel and Spakman (2000) is problematic, because these mechanisms do not explain the shape of the deep slab east of $\sim 17^\circ\text{E}$. Delamination (Bird, 1979) or Rayleigh–Taylor instability (Houseman and Molnar, 1997) could be more appropriate to explain the observed structure of the deep slab in the area of the Pannonian basin (Houseman et al., 2010).

According to our interpretation, the shallow slab under the Eastern Alps represents EU lower lithosphere delaminated and subducted during the post collision period since ~ 35 Ma. Some arguments for this interpretation were already presented in Brückl et al. (2010): 1) the upward directed jump from EU to AD Moho between 9°E and 14°E revealed by the seismic traverses EGT&NFP-20 (Valasek et al., 1991), TRANSALP (e.g., Kummerow et al., 2004; Lüschen et al., 2006), and Alp01 (Brückl et al., 2007); 2) the results of elastic plate modeling, indicating EU underthrusting AD; and 3) the close spatial relation of the axis of the shallow slab to the Moho fragmentation between AD

and EU. Our new tomographic model supports this interpretation because we observe the following: 1) a continuous change of dip of the shallow slab from steeply south dipping near the border between the Western and Eastern Alps to subvertical and steeply north dipping in the east under the Tauern window ($\sim 12^{\circ}\text{E}$ – 14°E); 2) the eastern termination of the shallow slab coincides approximately with the triple junction AD–EU–PA that represents the transition from convergence between AD and EU to lateral escape of PA to the east; and 3) the length of the subducted slab corresponds approximately with the post-collision convergence between AD and EU of about ~ 200 km (e.g., Frisch et al., 2000; Ustaszewski et al., 2008). There is also good agreement between the K-, L- and ALPASS-models regarding dip and extent of the shallow slab on the profiles P1 to P5 ($\sim 14^{\circ}\text{E}$) (Fig. 8).

An argument against a continuous EU slab below the Eastern Alps could be the reduced continuity at longitude $\sim 12^{\circ}\text{E}$. However, the deep slab, which extends from $\sim 13^{\circ}\text{E}$ further to the east may be connected to the shallow slab or interact with it in another manner, thus exerting an additional drag on the easternmost part of the shallow slab in that area. This finding from our new data could explain the reduced continuity of the Eastern Alps shallow slab and also the steep north dip at its eastern end.

7. Conclusions

The purpose of the ALPASS teleseismic project was to better understand the structure of the upper mantle in the area of the Eastern Alps and their surrounding tectonic provinces. Its main goal was to provide tomographic images of the shape, and ultimately the origin, of the lithospheric slab(s) below the Alpine orogen. Prior studies (Bijwaard et al., 1998; Piromallo and Morelli, 2003; Lippitsch et al., 2003; Koulakov et al., 2009) supplied valuable images of this and related structures. However, these results left room for fundamentally different interpretations in our area of interest. Thus the ALPASS experiment was undertaken, and the main features of the ALPASS tomographic model proved to be very robust and displayed no critical insensitivity to the choice of the inversion parameters or the few identified travel time outliers.

In our analysis, the ALPASS teleseismic model has been presented and interpreted employing depth slices (Fig. 7) and vertical profiles (Fig. 8). In the depth range of 60 km to 250 km, the most significant structure is a high velocity body that extends from the western border of the high resolution portion of the ALPASS-model ($\sim 9^{\circ}\text{E}$) to $\sim 15^{\circ}\text{E}$ in the east. This high velocity body, which we refer to as the “shallow slab”, follows the Moho fragmentation between Europe and Adria (Fig. 10). From west to east, the dip of the shallow slab changes continuously from $\sim 80^{\circ}$ south to subvertical or steeply dipping north. The eastern termination of the shallow slab coincides approximately with the bifurcation of the Moho fragmentation into EU–PA and AD–PA branches (Fig. 10). No further significant high velocity body was found eastward toward the Western Carpathians and below the northern Dinarides above 250 km depth. The Pannonian lithospheric fragment is underlain by relatively low velocities indicating high upper mantle temperatures in this area.

At greater depth, below 300 km, another significant west–east oriented high velocity body referred to as “deep slab” was imaged below the East Alps and the Pannonian fragment at $\sim 47^{\circ}\text{N}$ (Fig. 10). It begins in the west at $\sim 13^{\circ}\text{E}$ and extends to the vicinity of the eastern limit of resolution of the ALPASS-model. Profiles P4 and P5 (Fig. 8) show that there may be a connection of the deep slab to the shallow slab in this area. At greater depth (below 450 km) the deep slab continuously transitions into the “slab graveyard”, the well known high velocity area above the 670 km discontinuity in the wider Pannonian realm (e.g., Bijwaard et al., 1998; Piromallo and Morelli, 2003; Handy et al., 2010).

We interpret the deep slab to be subducted lithosphere of the Alpine Tethys (Penninic Ocean) which broke off after collision between AD and EU around 30 Ma ago (e.g., Wortel and Spakman, 2000). The shallow slab is interpreted as continental European lower lithosphere, which was delaminated and subducted during ongoing convergence between Adria and Europe after collision. The main arguments for this interpretation of the shallow slab as European lower lithosphere are its good fit to the southern end of the European Moho and its continuity from near the boundary of the Western and Eastern Alps to its eastern termination. The new ALPASS-model, supported by the teleseismic models of Koulakov et al. (2009) and Dando et al. (2011) does not indicate a change of subduction polarity from EU below AD in the west to AD below EU in the east as proposed by Lippitsch et al. (2003) and later integrated into tectonic models (e.g., Schmid et al., 2004).

The analysis of active tectonics in the Eastern Alps (Brückl et al., 2010) showed that convergence is still active between AD and EU, but ongoing lateral extrusion (Ratschbacher et al., 1991a,b) is the main process affecting the Pannonian fragment. Lateral extrusion of parts of the Eastern Alps and the Pannonian realm initiated in Upper Oligocene and Lower Miocene, and we assume that the crustal boundaries EU–PA and AD–PA were generated or became active at that time as mainly strike slip boundaries with only minor thrust components. Therefore, no or no substantial slab was generated and subducted at the EU–PA Moho boundary from the triple junction to the Western Carpathians and at the AD–PA boundary north of about 45°N . Further south, the thrust component of the relative velocity between Adria and the Dinarides increases substantially, and a shallow slab has been generated, as shown by images of large scale teleseismic models (e.g., Koulakov et al., 2009; Piromallo and Morelli, 2003).

Acknowledgments

We gratefully acknowledge the funding of the ALPASS project by the Austrian Academy of Sciences. A portion of the equipment used in the ALPASS experiment came from the IRIS/PASSCAL Instrument Center that is supported by the U.S. National Science Foundation. We thank the BOHEMA Working Group, especially Jaroslava Plomerová and Vladislav Babuška for the good cooperation concerning mutual data exchange. We further extend our thanks to Johanna Brückl for preparing the tectonic map and graphic presentation of the results.

References

- Babuška, V., Plomerová, J., Vecsey, L., Jedlička, P., Růžek, B., 2005. Ongoing passive seismic experiments unravel deep lithosphere structure of the Bohemian Massif. *Stud. Geophys. Geod.* 49, 423–430.
- Behm, M., Brückl, E., Chwatal, W., Thybo, H., 2007. Application of stacking techniques to 3D wide-angle reflection and refraction seismic data of the Eastern Alps. *Geophys. J. Int.* 170, 275–298. doi:10.1111/j.1365-246X.2007.03393.x.
- Bird, P., 1979. Continental delamination and the Colorado Plateau. *J. Geophys. Res.* 84, 7561–7571.
- Bijwaard, H., Spakman, W., Engdahl, E.R., 1998. Closing the gap between regional and global travel time tomography. *J. Geophys. Res.* 103, 30 055–30 078.
- Brückl, E., Bleibinhaus, F., Gosar, A., Grad, M., Guterich, A., Hrubcova, P., Keller, R., Majdanskí, M., Sumanovac, F., Tiira, T., Yliniemi, J., Hegedüs, E., Thybo, H., 2007. Crustal structure due to collisional and escape tectonics in the Eastern Alps region based on profiles Alp01 and Alp02 from the ALP 2002 seismic experiment. *J. Geophys. Res.* 112, B06308. doi:10.1029/2006JB004687.
- Brückl, E., Behm, M., Decker, K., Grad, M., Guterich, A., Keller, G.R., Thybo, H., 2010. Crustal structure and active tectonics in the Eastern Alps. *Tectonics* 29, TC2011. doi:10.1029/2009TC002491.
- Dando, B., 2010. Seismological structure of the Carpathian–Pannonian region in central Europe. Ph.D. Thesis, School of Earth and Environment, University of Leeds.
- Dando, B.D.E., Stuart, G.W., Houseman, G.A., Hegedüs, E., Brückl, E., Radovanović, S., 2011. Teleseismic tomography of the mantle in the Carpathian–Pannonian region of central Europe. *Geophys. J. Int.* 186, 11–31. doi:10.1111/j.1365-246X.2011.04998.x.
- Decker, K., Peresson, H., 1996. Tertiary kinematics in the Alpine–Carpathian–Pannonian system: links between thrusting, transform faulting and crustal extension. In: Wessely, G., Liebl, W. (Eds.), *Oil and Gas in Alpidic Thrustbelts and Basins of Central and Eastern Europe*: EAGE, Spec. Publ., 5, pp. 69–77.

- de Kool, M., Rawlinson, N., Sambridge, M., 2006. A practical grid based method for tracking multiple refraction and reflection phases in 3D heterogeneous media. *Geophys. J. Int.* 167, 253–270.
- Dewey, J.F., Pitman III, W.C., Ryan, W.B.F., Bonnin, J., 1973. Plate tectonics and the evolution of the Alpine system. *Geol. Soc. Am. Bull.* 84, 3137–3180.
- Doglion, C., Carminati, E., 2002. The effects of four subductions in NE Italy. *Mem. Sci. Geol.* 54, 1–4 ISSN 0391–8602.
- Frisch, W., Dunkl, I., Kuhlemann, J., 2000. Post-collisional orogen-parallel large-scale extension in the Eastern Alps. *Tectonophysics* 327 (Issues 3–4), 239–265.
- Grad, M., Guterch, A., Keller, G.R., Janik, T., Hegedüs, E., Vozár, J., Slaczka, A., Tiira, T., Yliniemi, J., 2006. Lithospheric structure beneath trans-Carpathian transect from Precambrian platform to Pannonian basin—CELEBRATION 2000 seismic profile CEL05. *J. Geophys. Res.* 111, B03301. doi:10.1029/2005JB003647.
- Grad, M., Tiira, T., ESC Working Group, 2009a. The Moho depth map of the European Plate. *Geophys. J. Int.* 176, 279–292. doi:10.1111/j.1365-246X.2008.03919.x.
- Grad, M., Brückl, E., Majdanski, M., Behm, M., Guterch, A., CELEBRATION 2000, ALP 2002 Working Groups, 2009b. Crustal structure of the Eastern Alps and their foreland: seismic model beneath the CEL10/Alp04 profile and tectonic implications. *Geophys. J. Int.* 177, 279–295. doi:10.1111/j.1365-246X.2008.04074.x.
- Geissler, W., Kind, R., Yuan, X., 2008. Upper mantle and lithospheric heterogeneities in central and eastern Europe as observed by teleseismic receiver functions. *Geophys. J. Int.* 174, 351–376. doi:10.1111/j.1365-246X.2008.03767.x.
- Grenerczy, G., Kenyeres, A., 2006. Crustal deformation between Adria and the European platform from space geodesy. In: Pinter, N., Grenerczy, Weber, J., Stein, S., Medak, D. (Eds.), *The Adria microplate: GPS geodesy, tectonics and hazards*. NATO Science Series IV: Earth and Environmental Sciences, 61. Springer, pp. 321–334.
- Guterch, A., Grad, M., Špičák, A., Brueckl, E., Hegedus, E., Keller, G.R., Thybo, H., CELEBRATION, 2000, ALP 2002, SUDETES 2003 Working Groups, 2003. An overview of recent seismic refraction experiments in Central Europe. *Stud. Geophys. Geod.* 47, 651–657.
- Handy, M., Schmid, S., Bousquet, R., Kissling, E., Bernoulli, D., 2010. Reconciling plate-tectonic reconstructions of Alpine Tethys with the geological–geophysical record of spreading and subduction in the Alps. *Sci. Rev.* doi:10.1016/j.earscirev.2010.06.002.
- Hearn, T., Ni, J., 1994. Pn velocities beneath continental collision zones: the Turkish–Iranian Plateau. *Geophys. J. Int.* 117, 273–283.
- Horváth, F., Bada, G., Szaifán, P., Tari, G., Ádám, A., Cloetingh, S., 2006. Formation and deformation of the Pannonian basin: constraints from observational data. In: Gee, D.G., Stephenson, R.A. (Eds.), *European Lithosphere Dynamics*, 32. Geological Society London Memoir, London, pp. 129–145.
- Houseman, G., Stuart, G., Dando, B., Hetenyi, G., Lorinczi, P., Hegedues, E., Brückl, E., 2010. Lithospheric convergence preceded extension in the Pannonian–Carpathian system. *Geophys. Res. Abstr.* 12 EGU2010-12232-3, EGU General Assembly.
- Houseman, G., Molnar, P., 1997. Gravitational (Rayleigh–Taylor) instability of a layer with non-linear viscosity and convective thinning of continental lithosphere. *Geophys. J. Int.* 128, 125–150.
- Hrubcova, P., Šroda, P., Spicák, A., Guterch, A., Grad, M., Keller, G.R., Brückl, E., Thybo, H., 2005. Crustal and uppermost mantle structure of the Bohemian Massif based on CELEBRATION 2000 data. *J. Geophys. Res.* 110 (B11305). doi:10.1029/2004JB003080.
- Hrubcova, P., Šroda, P., CELEBRATION 2000 Working Group, 2008. Crustal structure at the easternmost termination of the Variscan belt based on CELEBRATION 2000 and ALP 2002 data. *Tectonophysics* 460, 55–75.
- Kennett, B.L.N., Engdahl, E.R., Buland, R., 1995. Constraints on seismic velocities in the Earth from travel times. *Geophys. J. Int.* 122, 108–124.
- Kissling, E., Schmid, S.M., Lippitsch, R., Ansorge, J., Fügenschuh, B., 2006. Lithosphere structure and tectonic evolution of the Alpine arc: new evidence from high-resolution teleseismic tomography. In: Gee, D.G., Stephenson, R.A. (Eds.), *European Lithosphere Dynamics*, 32. Geological Society Memoir, London, pp. 29–145.
- Koulakov, I., Kaban, M.K., Tesauero, M., Cloetingh, S., 2009. P- and S-velocity anomalies in the upper mantle beneath Europe from tomographic inversion of ISC data. *Geophys. J. Int.* 179, 345–366.
- Kummerow, J., Kind, R., Oncken, O., Giese, P., Tyberg, T., Wylegalla, K., Scherbaum, F., TRANSALP Working Group, 2004. A natural and controlled source seismic profile through the Eastern Alps: TRANSALP. *Earth Planet. Sci. Lett.* 225, 115–129.
- Lammerer, B., Weger, M., 2008. A crustal-scale cross section through the Tauern Window (eastern Alps) from geophysical and geological data. In: Siegesmund, S., et al. (Ed.), *Tectonic Aspects of the Alpine–Dinaride–Carpathian System: Geological Society, London, Special Publications*, 298, pp. 219–229.
- Le Pichon, X., Bergerat, F., Roulet, M.-J., 1988. Plate kinematics and tectonics leading to the Alpine belt formation: a new analysis. In: Clark, S.P., Burchfiel, B.C., Suppe, J. (Eds.), *Processes in Continental Lithospheric Deformation: GSA, Special Paper*, 218, pp. 111–131.
- Linzer, H.-G., Decker, K., Peresson, H., Dell’Mour, R., Frisch, W., 2002. Balancing lateral orogenic float of the Eastern Alps. *Tectonophysics* 354, 211–237.
- Lippitsch, R., Kissling, E., Ansorge, J., 2003. Upper mantle structure beneath the Alpine orogen from high-resolution teleseismic tomography. *J. Geophys. Res.* 108, 2376. doi:10.1029/2002JB002016.
- Lüschen, E., Borrini, D., Gebrande, H., Lammerer, B., Millahn, K., Neubauer, F., Nicolich, R., TRANSALP Working Group, 2006. TRANSALP-deep crustal Vibroseis and explosive seismic profiling in the Eastern Alps. *Tectonophysics* 414 (1–4), 9–38.
- Moores, E.M., Twiss, R.J., 1995. *Tectonics*. W. H. Freeman, New York, p. 415.
- Pamić, J., Tomljenović, B., Balen, D., 2002. Geodynamic and petrogenetic evolution of Alpine ophiolites from the central and NW Dinarides: an overview. *Lithos* 65, 113–142.
- Piomallo, C., Morelli, A., 2003. P wave tomography of the mantle under the Alpine–Mediterranean area. *J. Geophys. Res.* 108 (B2). doi:10.1029/2002JB001757.
- Ratschbacher, L., Merle, O., Davy, P., Cobbold, P., 1991a. Lateral extrusion in the Eastern Alps, Part 1: boundary conditions and experiments scaled for gravity. *Tectonics* 10 (2), 245–256.
- Ratschbacher, L., Frisch, W., Linzer, H.G., Merle, O., 1991b. Lateral extrusion in the Eastern Alps, Part 2: structural analysis. *Tectonics* 10 (2), 257–271.
- Rawlinson, N., Kennett, B.L.N., 2004. Rapid estimation of relative and absolute delay times across a network by adaptive stacking. *Geophys. J. Int.* 157, 332–340.
- Rawlinson, N., Reading, A.M., Kennett, B.L.N., 2006. Lithospheric structure of Tasmania from a novel form of teleseismic tomography. *J. Geophys. Res.* 111, B02301. doi:10.1029/2005JB003803.
- Rawlinson, N., Kennett, B.L.N., 2008. Teleseismic tomography of the upper mantle beneath the southern Lachlan Orogen, Australia. *Phys. Earth Planet. Inter.* 167, 84–97.
- Royden, L.H., 1993. Evolution of retreating subduction boundaries formed during continental collision. *Tectonics* 12, 629–638.
- Schmid, S.M., Fügenschuh, B., Kissling, E., Schuster, R., 2004. Tectonic map and overall architecture of the Alpine orogen. *Eclogae Geol. Helv.* 97, 93–117.
- Schmid, S.M., Bernoulli, D., Fügenschuh, B., Matenco, L., Schuster, R., Schefer, S., Tischler, M., Ustaszewski, K., 2008. The Alpine–Carpathian–Dinaridic orogenic system: correlation and evolution of tectonic units. *Swiss J. Geosci.* 101 (1), 139–183.
- Stampfli, G.M., Kozur, H.W., 2006. Europe from the Variscan to the Alpine cycles. In: Gee, D.G., Stephenson, R.A. (Eds.), *European Lithosphere Dynamics*, 32. Geol. Soc. London, Memoir, London, pp. 129–145.
- Šumanovac, F., Orešković, J., Grad, M., ALP2002 Working Group, 2009. Crustal structure at the contact of the Dinarides and Pannonian basin based on 2-D seismic and gravity interpretation of the Alp07 profile in the ALP2002 experiment. *Geophys. J. Int.* 179, 615–633. doi:10.1111/j.1365-246X.2009.04288.x.
- Šumanovac, F., 2010. Lithosphere structure at the contact of the Adriatic microplate and the Pannonian segment based on the gravity modelling. *Tectonophysics* 485, 94–106. doi:10.1016/j.tecto.2009.12.005.
- Tackley, P. J., in press. Living dead slabs in 3-D: The dynamics of compositionally-stratified slabs entering a ‘slab graveyard’ above the core–mantle boundary. *Phys. Earth Planet. Inter.*, doi:10.1016/j.pepi.2011.04.013.
- Ustaszewski, K., Schmid, S.M., Fügenschuh, B., Tischler, M., Kissling, E., Spakman, W., 2008. A map-view restoration of the Alpine–Carpathian–Dinaridic system for the Early Miocene. *Swiss J. Geosci.* 101 (Supplement 1), 273–294.
- Valasek, P., Mueller, St. Frei, W., Holliger, K., 1991. Results of NFP20 seismic reflection profiling along the Alpine section of the European Geotraverse (EGT). *Geophys. J. Int.* 105, 85–102.
- Waldhauser, F., Kissling, E., Ansorge, J., Mueller, St. 1998. Three-dimensional interface modelling with two-dimensional seismic data: the Alpine crust–mantle boundary. *Geophys. J. Int.* 135, 264–278.
- Waldhauser, F., Lippitsch, R., Kissling, E., Ansorge, J., 2002. High-resolution teleseismic tomography of upper mantle structure using an a priori 3D crustal model. *Geophys. J. Int.* 150, 1–12.
- Wortel, M.J.R., Spakman, W., 2000. Subduction and slab detachment in the Mediterranean–Carpathian region. *Science* 290 (5498), 1910–1917.